LANGMUIR
Cite This: *Langmuir* 2019, 35, 709−717
Article
pubs.acs.org/Langmuir

# On the Stability of Polymeric Nanoparticles Fabricated through Rapid Solvent Mixing

Tatiana I. Morozova,[†] Victoria E. Lee,[‡] Athanassios Z. Panagiotopoulos,[‡] Robert K. Prud'homme,[‡] Rodney D. Priestley,[‡] and Arash Nikoubashman*[,†]

[†]Institute of Physics, Johannes Gutenberg University Mainz, Staudingerweg 7, 55128 Mainz, Germany
[‡]Department of Chemical and Biological Engineering, Princeton University, Princeton, New Jersey 08544, United States

**ABSTRACT:** We study the stability of polymeric nanoparticles fabricated through the rapid mixing of polymers in a good solvent with a poor solvent that is miscible with the good solvent. In previous experiments where water was used as the poor solvent, a negative surface charge was measured on the precipitated nanoparticles, which led to the long-time stability of the dispersion. It was argued that these charges originate presumably from either water or hydroxide adsorption at the hydrophobic nanoparticle surface or from impurities in the feed streams that preferentially adsorb on the precipitated nanoparticles. To elucidate the origin of this stabilization mechanism, we performed experiments wherein we replaced water with a nonpolar poor solvent. The polymers aggregated into stable nanoparticles for a range of processing parameters. We investigated theoretically three possible explanations for this stability, i.e., electrostatic stabilization, conditional thermodynamic equilibrium, and steric stabilization. Our experiments and considerations suggest that steric stabilization is the most likely candidate.

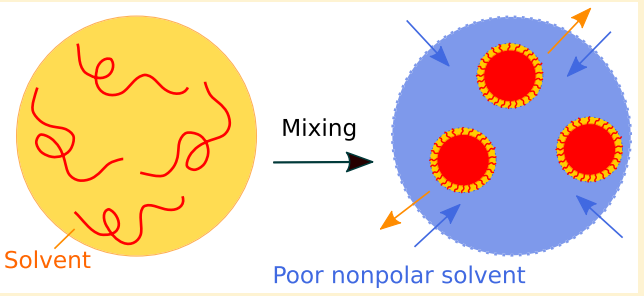




## INTRODUCTION

Polymeric nanoparticles (NPs) are widely used in different scientific and industrial areas, such as biomedical drug delivery applications,[1,2] cosmetics,[3,4] interfacial property modifiers in enhanced oil recovery,[5] and printing inks.[6] This broad scope of applications is achieved by exploiting a large variety of NP structures and material properties. Typically, NPs are fabricated in solution, e.g., through nanoemulsion polymerization,[7] self-organized precipitation,[8] or flash nanoprecipitation (FNP).[9] The resulting NPs are then kept in solution or dried to a powder for storage until they get redispersed in a suitable solvent.

To ensure a long shelf life of these colloidal dispersions, a high stability against aggregation is desirable. There are two main mechanisms for achieving stability in colloidal dispersions, namely, electrostatic stabilization and steric stabilization. The former is based on the mutual repulsion of like electrical charges and can be described by the well-known Derjaguin−Landau−Verwey−Overbeek (DLVO) theory.[10,11] This theory characterizes the forces between charged surfaces interacting through a liquid medium, and it is usually applied to aqueous suspensions, wherein electrostatic mechanisms are screened and the structure of the counterion double layer is well understood. In contrast, its application in nonaqueous dispersions is rather limited, because the origin of the surface charge, the structure of the double layer, and the meaning of the shear plane are less clear.[12] In DLVO theory, there are two main forces acting on the colloidal particles: attractive van der Waals (VDW) forces, originating from (spontaneous)dipole−dipole interactions, and repulsive electrostatic forces, emerging from the overlapping electrical double layers that surround the dispersed particles in the medium. The interplay between these two forces dictates the colloidal stability. In this context, one parameter that is often used to quantify stability is the $\zeta$ potential, which is defined as the electric potential at the slipping plane of the NP (the boundary of the surrounding liquid layer attached to the moving particles in the medium). As a rule of thumb, the dispersion becomes more stable with increasing $\zeta$ potential and values of $|\zeta| \gtrsim 30$ mV are sufficient in most cases to achieve moderate stability.[13,14]

Polymer steric stabilization of colloidal dispersions is achieved by having solvated polymer chains on the colloidal surface. Under good solvent conditions, excluded volume effects create repulsive interactions as two colloids approach distances that require compression of the surface polymer chains. The competition between this repulsive interaction and attractive VDW attraction can create a barrier larger than the thermal energy at some distance from contact, which can impart colloidal stability.

Alternatively, a stable colloidal system can be achieved when the aggregation and dissociation processes are balanced,[15] i.e., the free energy of the system is minimized at a state where a fraction of the polymers is aggregated and the remainder coexists as collapsed globules in solution. This scenario has

**Received:** October 9, 2018
**Revised:** December 10, 2018
**Published:** December 28, 2018




DOI: 10.1021/acs.langmuir.8b03399
*Langmuir* 2019, 35, 709−717

been termed conditional thermodynamic equilibrium and is reminiscent of the self-assembly of amphiphiles into micelles,[16,17] wherein above the critical micelle concentration, aggregates start to form in solution coexisting with free unassociated amphiphiles.

It is clear that the physical mechanisms responsible for colloidal stability depend strongly on the specific composition of the NPs. In this work, we concentrate on the FNP technique, wherein polymers in a good solvent are rapidly mixed with a poor solvent (typically water), which is miscible with the good solvent, leading to polymer supersaturation and aggregation into NPs. Figure 1 shows a schematic illustration

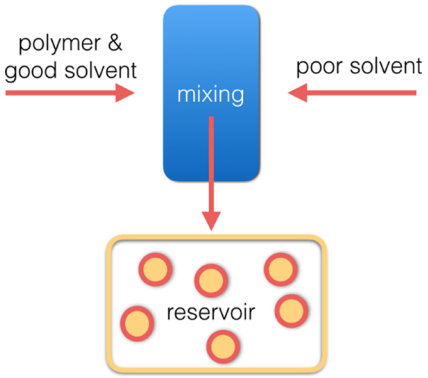


**Figure 1.** Schematic representation of the FNP mixing process.

of the experimental setup. FNP was successfully employed for encapsulating hydrophobic materials,[18−20] fabricating homogeneous NPs,[14,21] core−shell and Janus particles,[22,23] and NPs with even more complex internal structures.[24] In most of these cases, colloidal stability was achieved through surface adsorption of amphiphilic polymers that act as a steric barrier[18−20] or by using polymers with charged end groups.[21]

Surprisingly, in several studies,[14,22−24] the precipitated NPs were found to be stable even though no amphiphilic stabilizer was incorporated in the formulation. The polymers comprising the core had no ionizable groups, but the $\zeta$ potential of polystyrene (PS) and polyisoprene NPs precipitated in a tetrahydrofuran (THF)−water mixture was determined as $\zeta \approx -30$ mV, almost independent of the NP size (radii ranging from 45 to 135 nm).[14] The physical origin of this negative surface charge is still elusive, but previous experiments of air bubbles and oil droplets in water suggest that the measured $\zeta$ potential is the result of water in the FNP experiments;[25−31] e.g., it was argued that the adsorption of hydroxide ions on the hydrophobic surface results in a negative surface charge[26,31] or that adsorption of bicarbonate ions from the equilibrium between $CO_2$ in air and the water causes charging.[32]

To elucidate the role of water and the physical phenomena responsible for the observed electrostatic stabilization of FNP in aqueous media, we performed FNP experiments wherein we replaced water with a nonpolar poor solvent. To our surprise, we were still able to produce stable colloidal dispersions for a wide range of process parameters. We then assessed theoretically three possible mechanisms responsible for this stability, i.e., electrostatic stabilization, conditional thermodynamic equilibrium, and steric stabilization, and concluded that the latter scenario is the most likely.

## EXPERIMENTAL SECTION

We used PS in all our experiments, as this polymer is readily available and its physical properties are well understood and documented in the literature. We used either THF or toluene as the good solvent. For the poor solvent in our experiments, we chose the nonpolar compounds hexane and heptane, which are both miscible with THF and toluene. FNP was performed at room temperature ($T \approx 298$ K) using a multi-inlet vortex mixer and a confined impinging jet mixer. In both mixers, the polymer solution was injected against an equal volume of the poor solvent. The effluent stream fell into a reservoir, containing the same poor solvent as that used in the feed stream. We systematically varied the volume ratio between the feed streams and the reservoir, (polymer solution)/(poor solvent)/(poor solvent in the reservoir), using 1:1:0, 1:1:1, 1:1:2.5, 1:1:5, and 1:1:10. We were able to obtain reliable size measurements from dynamic light scattering (DLS) only for a 1:1:1 ratio, containing 1/3 good solvent and 2/3 poor solvent. Therefore, all subsequent experiments have been conducted at a 1:1:1 ratio.

We first conducted FNP with PS dissolved in THF using hexane as a poor solvent for two polymer concentrations in the feed stream, namely, $C_{PS} = 0.1$ and 0.5 mg/mL. DLS measurements of the samples revealed an average particle radius of $R = 105 \pm 30$ nm for the lower polymer concentration and $R = 200 \pm 50$ nm for the higher one, which is consistent with the dependence $R \propto C^{1/3}$ observed in previous experiments and simulations.[14] Figure 2 shows the evolution of $R$ as a function of time, and it is clear that the NP dispersions were stable for at least 10 days.

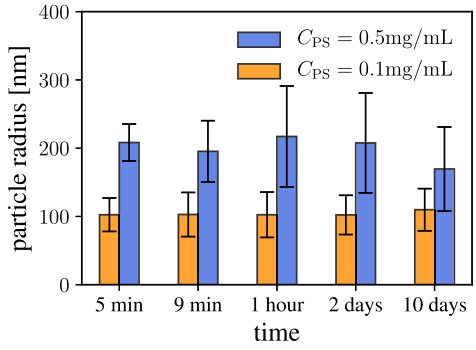


**Figure 2.** Mean NP radii for PS in THF−hexane mixtures at two polymer concentrations in the feed stream $C_{PS} = 0.1$ and 0.5 mg/mL vs time after FNP.

We then performed a second set of experiments, where we used toluene as a good solvent, since THF might adsorb water from the air and thus could introduce undesired water into the system. We conducted FNP experiments using a polymer concentration of $C_{PS} = 0.1$ mg/mL, and were able to prepare stable NP dispersions. The average particle radius was $R = 120 \pm 33$ nm, which is close to the value for NPs prepared using THF as a good solvent. Figure 3 shows a comparison of the mean NP sizes prepared using THF or toluene as a good solvent.

To measure possible trace amounts of water in our samples, we performed a Karl Fischer (KF) analysis to determine moisture content. We found a water concentration of $C_W = 0.23$ wt % in pure THF and $C_W = 0.03$ wt % in pure toluene. No measurable water was found in pure hexane.

To better understand the origin of the colloidal stability, we subsequently evaporated the good solvent from the mixtures. The boiling points of THF and hexane are very close to each other (339 K and 342 K, respectively) whereas the boiling point of toluene (384 K) is higher than that of hexane, rendering the evaporation of only the good solvent technically infeasible. There are two possible solutions to this problem: (i) using a good solvent with a lower boiling point than that of hexane, e.g., dichloromethane (313 K) or (ii) using a poor solvent with a higher boiling point than that of THF (or toluene), e.g., heptane (371 K) or octane (398 K). We chose the second route, since



DOI: 10.1021/acs.langmuir.8b03399
Langmuir 2019, 35, 709−717

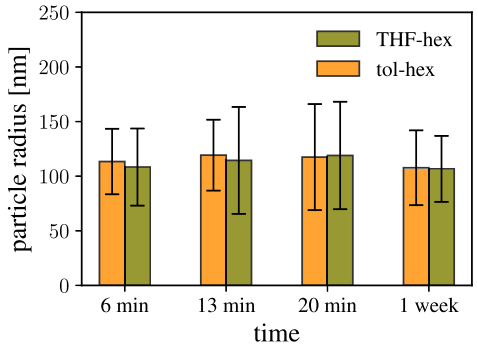


**Figure 3.** Mean NP radii for PS in THF−hexane and toluene−hexane mixtures ($C_{PS}$ = 0.1 mg/mL) vs time after FNP.

heptane and octane have chemical structures similar to that of hexane, and hence this replacement should not significantly influence the FNP results. We conducted FNP experiments with PS dissolved in THF against heptane, using a 1:1:1 ratio and two polymer concentrations: $C_{PS}$ = 0.1 and 0.5 mg/mL. We determined the size of the precipitated NPs using DLS and found average NP radii of $R$ = 110 ± 40 and 230 ± 40 nm for $C_{PS}$ = 0.1 and 0.5 mg/mL, respectively, which are similar to the values obtained for the THF−hexane and toluene−hexane mixtures (cf. Figure 3). A transmission electron microscopy (TEM) image of the colloidal suspension for polymer concentration in the feed stream $C_{PS}$ = 0.5 mg/mL is shown in Figure 4. Figure 5 shows

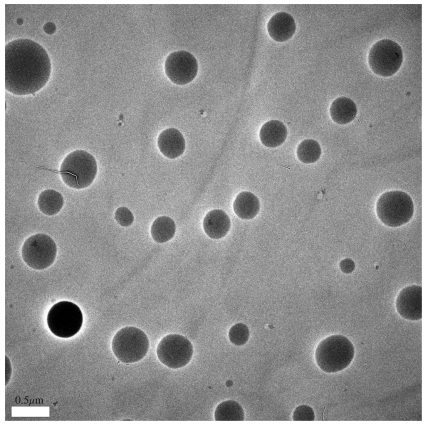


**Figure 4.** TEM image of the PS nanoparticles formed via FNP in THF−heptane mixture. The polymer concentration in the feed stream was $C_{PS}$ = 0.5 mg/mL. The scale bar in the image indicates 0.5 μm.

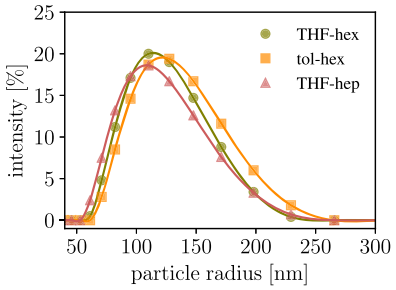


**Figure 5.** Comparison of NP radius distributions for PS in THF−hexane, in toluene−hexane, and in THF−heptane mixtures. DLS measurements were taken 12 min after the suspensions were prepared.

the size distributions of the NPs measured shortly after the FNP experiments, which are almost identical for the various choices of good and poor solvents. These findings can be rationalized by considering the similarity of the Hamaker constants for PS in these mixtures.

The resulting particle dispersion was next placed under vacuum on a rotary evaporator for 90 min to remove residual THF, and we then measured again the size distribution using DLS. The resulting system was unstable.

Before evaporating the residual solvent, we attempted to measure the ζ potential. However, we were unable to obtain reliable and consistent results, as our measurements suffered from broad distributions, different mean values, and inconsistent signs of the ζ potential. Such complications are not uncommon for colloidal dispersions in nonaqueous media and originate from their low conductivity. We measured a conductivity of $3.3 \times 10^{-7}$ S/cm for our samples, which is 2 orders of magnitude smaller than typical values determined for aqueous media.[33] Such small conductivities have also been reported by Xu et al. for carbon black in low polar media.[34] In that work, similar complications were encountered for determining the ζ potential, resulting in large measurement uncertainties.

## THEORETICAL CONSIDERATIONS ON PARTICLE STABILITY

In this section, we will rationalize potential mechanisms for the particle stability observed in the experiments. If not stated otherwise explicitly, we will focus on systems with a mixing ratio of 1:1:1 polymer concentrations in the feed stream of $C_{PS}$ = 0.1 mg/mL, in THF/toluene−hexane or THF−heptane mixtures.

Colloidal particles in solution naturally attract each other due to dipole−dipole interactions. The VDW interaction between two spheres of radius $R_1$ and $R_2$ can be calculated[35]

$$U_{VDW}(h, R_1, R_2) = -\frac{A}{6}\left[\left(\frac{2R_1R_2}{(h + R_1 + R_2)^2 - (R_1 + R_2)^2}\right) + \frac{2R_1R_2}{(h + R_1 + R_2)^2 - (R_1 - R_2)^2} + \ln\left(\frac{(h + R_1 + R_2)^2 - (R_1 + R_2)^2}{(h + R_1 + R_2)^2 - (R_1 - R_2)^2}\right)\right] \quad (1)$$

where $A$ is the Hamaker constant and $h$ is the surface-to-surface distance. To estimate the typical attraction strengths in the experimental systems, we consider the VDW interactions between two PS NPs in a mixture of a poor solvent (hexane or heptane) and a good solvent (THF or toluene). We compute the Hamaker constants for these systems through the Lifshitz theory,[36,37] in which the Hamaker constant of a material is related to the dielectric decay function. Following the assumptions made in ref 16, we can approximate the Hamaker constant for the symmetric case, wherein identical phases 1 interact across medium 3

$$A_{131} = \frac{3}{4}k_BT\left(\frac{\varepsilon_1 - \varepsilon_3}{\varepsilon_1 + \varepsilon_3}\right)^2 + \frac{3\hbar\omega_e}{16\sqrt{2}}\frac{(n_1^2 - n_3^2)^2}{(n_1^2 + n_3^2)^{3/2}} \quad (2)$$

where $\varepsilon_1$ and $\varepsilon_3$ and $n_1$ and $n_3$ are the dielectric constants and refractive indexes of medium 1 and 3, respectively. The main electronic absorption frequency $\nu_e = 2\pi\omega_e$ was assumed to be $\nu_e = 3 \times 10^{15}$ s$^{-1}$ for all media.[16] The values for the dielectric constants and refractive indexes are given in Table 1.

For PS in pure hexane, the case with the strongest attraction, eq 2 can be directly used to estimate the strength of the VDW interaction. Here, we find $A_{131} = 0.92 \times 10^{-20}$ J, which is close to the experimental values for PS in water ($0.95-1.3 \times 10^{-20}$



DOI: 10.1021/acs.langmuir.8b03399
Langmuir 2019, 35, 709−717

**Table 1. Dielectric Constant, $\varepsilon$, and Refractive Index, $n$, of the Chemical Compounds Used in the FNP System**

| | $\varepsilon$ | $n$ |
|---|---|---|
| PS | 2.55[16] | 1.56[16] |
| hexane | 1.89[38] | 1.37[39] |
| heptane | 1.90[40] | 1.39[39] |
| THF | 7.6[41] | 1.41[39] |
| toluene | 2.30[38] | 1.49[42] |

J),[16] another poor solvent for PS. To estimate the VDW interactions in the mixtures of good and poor solvents, we first need to determine the corresponding dielectric constants and refractive indexes. The dielectric constant for a toluene−hexane mixture with a mole fraction of hexane $X_{hex} = 0.65$ has been determined experimentally[38] as $\varepsilon_{tol-hex} = 2.01$. The refractive index of the mixture can be estimated via

$$n_{A-B} \simeq X_A^2 n_A + 2X_A X_B (n_A n_B)^{1/2} + X_B^2 n_B \quad (3)$$

leading to $n_{tol-hex} = 1.38$. The corresponding Hamaker constant for PS in the toluene−hexane mixtures is then $A_{131} = 0.81 \times 10^{-20}$ J.

For the THF−hexane/heptane mixtures, the experimental values for the refractive indexes are known from the literature, i.e., $n_{THF-hex} = 1.38$,[39,43] and $n_{THF-hep} = 1.39$,[39] respectively. We estimate the dielectric constant of the mixtures using[44]

$$\frac{\varepsilon_{A-B} - 1}{\varepsilon_{A-B} + 2} = X_A \frac{\varepsilon_A - 1}{\varepsilon_A + 2} + X_B \frac{\varepsilon_B - 1}{\varepsilon_B + 2} \quad (4)$$

yielding $\varepsilon_{THF-hex} = 2.82$ and $\varepsilon_{THF-hep} = 2.83$. With these values, we obtain the Hamaker constants $A_{131} = 0.82 \times 10^{-20}$ J for the NP−NP interaction in the THF−hexane mixture, and $A_{131} = 0.73 \times 10^{-20}$ J in the THF−heptane mixture, which are similar to that for the toluene−hexane mixture and slightly smaller than the value computed for pure hexane, as expected.

In the experiments, the average radius of precipitated PS NPs was $R \approx 110$ nm and the resulting VDW interactions are presented in Figure 6. We can see that the attraction is strongest for the NP−NP pair in pure hexane. The attraction between NPs is somewhat weaker in the solvent mixtures, but it is still sufficiently strong to drive aggregation. However, since we observe stable colloidal dispersions in the experiments under these processing conditions, there must be some stabilization mechanism at play that counteracts the attractive VDW forces. We will discuss potential candidates in the subsequent sections.

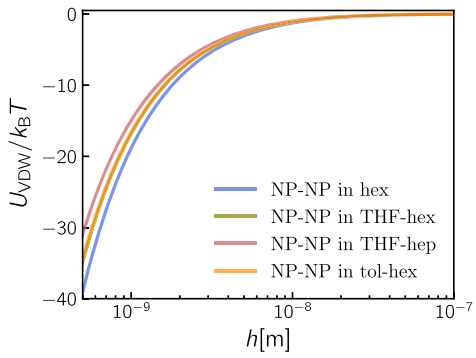


**Figure 6.** Van der Waals interaction in the FNP system between two precipitated NPs, $R = 110$ nm, for various solvent compositions, as indicated. The curves for the THF−hexane and toluene−hexane mixtures are almost indistinguishable.

**Electrostatic Stabilization.** Colloidal stability can be achieved through long-ranged electrostatic repulsion between the NPs, which balances out the short ranged VDW attraction. In a colloidal dispersion, NP surface charge can stem from the colloids themselves, e.g., by precipitating polymers with charged end groups[21] or from additional ionic species in the system, e.g., surfactants,[45,46] surface ionic group dissociation, or electron transfer between molecules of the medium and the surface of the NPs.[34] Experimentally, we were unable to support or exclude electrostatic stabilization, since all $\zeta$ potential measurements were unreliable.

Despite the experimental challenges, we can still estimate the $\zeta$ potential that would be required to stabilize the NPs. For a nonpolar liquid, the dielectric constant is low, e.g., $\varepsilon_{hex} = 1.89$ for hexane, and the resulting Debye length is a few micrometers. In such a case, the electrostatic interactions can be described using a Coulombic potential. Then, the total interaction between two charged NPs is given by the sum of the VDW attraction and the electrostatic repulsion[47,48]

$$U_{tot} = \frac{4\pi\varepsilon\varepsilon_0 R^2 \zeta^2}{h + 2R} + U_{VDW} \quad (5)$$

where $U_{VDW}$ is defined in eq 1. In Figure 7a, we have plotted $U_{tot}$ as a function of separation distance $h$ for different values of the $\zeta$ potential in the THF−hexane mixture. For neutral NPs, the VDW attraction is in the order of tens of $k_BT$ at nanometer separation and vanishes almost completely at $h$ in the order of micrometers. For charged NPs, there is a repulsive barrier at intermediate distances, which becomes more pronounced with increasing $\zeta$ potential and eventually exceeds the thermal energy $k_BT$ for $|\zeta| \gtrsim 30$ mV. In Figure 7b, we plotted $U_{tot}$ for different solvent conditions at $|\zeta| = 60$ mV, wherein the polymeric NPs should be stable (see the following discussion).

The stability of the NPs can be estimated via the so-called stability constant $W$,[10,15,48] which is the factor by which the rate of rapid flocculation is reduced due to interparticle forces. This quantity can be calculated through

$$W = 2R \int_{2R}^{\infty} \exp\left(\frac{U_{tot}}{k_BT}\right) \frac{dr}{r^2} \quad (6)$$

For the interactions at hand, the integral can be approximated to

$$W \approx \left(\frac{A_{131} k_B^2 T^2}{3072 \varepsilon^3 \varepsilon_0^3 R^3 \zeta^6}\right)^{1/4} \exp\left(\frac{2\pi\varepsilon\varepsilon_0 R \zeta^2}{k_BT}\right) \quad (7)$$

If $W \sim 10^5$, a colloidal system is considered to be stable and the value of the required $\zeta$ potential can be estimated[47]

$$\zeta^2 > \frac{10^3}{\varepsilon R} \quad (8)$$

where the $\zeta$ potential is in millivolts and the NP radius is in micrometers. To stabilize NPs with an average radius of $R = 110$ nm, the estimated value of the $\zeta$ potential should be at least 60 mV for the THF−hexane/heptane mixtures and at least 70 mV for the toluene−hexane mixture and for pure hexane (see Figure 8).

In hydrocarbon solutions the $\zeta$ potential may be equated with considerable accuracy to the surface potential.[47] To



DOI: 10.1021/acs.langmuir.8b03399
Langmuir 2019, 35, 709−717

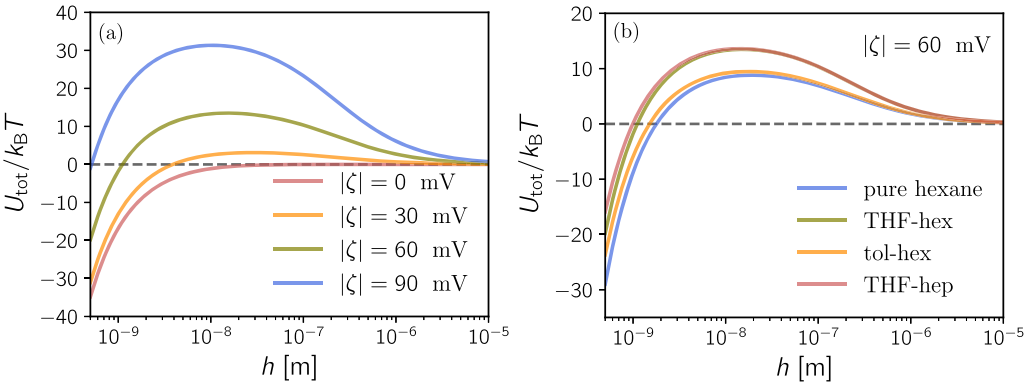


**Figure 7.** (a) Interaction potential between two PS NPs, $R$ = 110 nm, in the THF−hexane mixture as a function of particle separation distance $h$ for different $\zeta$ potentials. (b) Interaction potential between two PS NPs, $R$ = 110 nm, with $|\zeta|$ = 60 mV in four different solutions: pure hexane, THF−hexane, toluene−hexane, and THF−heptane.

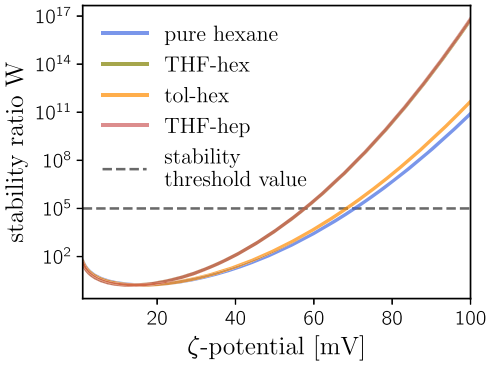


**Figure 8.** Stability constant $W$ for PS NPs with average radius $R$ = 110 nm in pure hexane, THF−hexane, toluene−hexane, and THF−heptane as a function of $\zeta$ potential.

calculate the charge of a sphere with the corresponding surface potential we used

$$Q = 4\pi\varepsilon_0\varepsilon\zeta R \tag{9}$$

which yields a value of $Q \approx 10e$ elementary charges for a PS NP with radius $R$ = 110 nm in the THF−hexane mixture. This finding is consistent with previous estimations for particle stabilization in nonpolar media.[34,49,50]

The final question is the origin of the charges, and we will consider several scenarios in the following. If we consider hydroxide ions of water as a potential source of the charge, then one water molecule in $10^7$ should dissociate and accumulate on the NP surface. According to our titration experiments, there are approximately $10^8$ water molecules per NP, providing a sufficient amount of water for charge dissociation, at least in principle. Recently, adsorption of bicarbonate ions ($HCO_3^-$) was proposed as an alternative explanation for the electrostatic stabilization of hydrophobic NPs in aqueous media;[32] indeed, even under inert conditions, carbon dioxide from the atmosphere is taken up by water into its carbonic acid $H_2CO_3$ form. For the trace amount of water in our systems with THF, we estimate 50 $HCO_3^-$ molecules per NP, assuming that the water in our system can be treated as a bulk medium.[32] To reach the charge required for stabilization ($Q \approx 10e$), every fifth carbonic acid should adsorb on the NP surface. However, spontaneous charge dissociation occurs much less frequently in nonpolar media compared to that in low-polar solvents with $\varepsilon \sim 10$.[51,52] Hence, ion dissociation in our systems seems quite unlikely and even if it could take place, it is unclear why the ions should be kept separated[53] and accumulate preferentially on the NP surface.

Another source for the charge could be the polymers themselves. The PS chains were synthesized by living ionic polymerization and terminated with hydrocarbons and thus should not carry any residual charges. However, it is conceivable that photodegradation or oxidation during storage impacted the purity of the PS chains.[54] Given that a NP with radius $R$ = 110 nm consists of approximately 165 000 polymer chains (see below) and that the charged end groups arrange most likely on the NP surface to maximize their mutual distance,[21] polymer impurities could be a possible explanation for charge stabilization of the NPs.

**Conditional Thermodynamic Equilibrium.** The long-term stability of a colloidal system can be described with the help of thermodynamics, i.e., by estimating the free energy of a system. There are two competitive processes in the system: aggregation and dissociation. It is possible that the free energy of the system is minimized at a state where polymeric aggregates and free chains coexist. To test whether such a picture holds true for our system, we determined its (approximate) free energy

$$F = U_{sys} - TS_{sys} \tag{10}$$

where $U_{sys}$ is the potential energy of the system and $S_{sys}$ is its entropy. In the experiments with polymer concentration $C_{PS}$ = 0.1 mg/mL at a 1:1:1 mixing ratio, there is roughly $V_{res}$ = 3 mL of liquid in the reservoir, whereas the total polymer volume is only in the order of $10^{-4}$ mL. Hence, we will use $V_{res}$ as the accessible volume, for the sake of simplicity.

To estimate the free energy of the system, we assume a uniform size distribution of NPs with radius $R$ = 100 nm (cf. Figure 5a). Further, we assume that globules consist of one collapsed PS chain and have a radius of $R_{gl} \approx 2$ nm. These approximations are consistent with our experiments and previous simulations,[14] wherein we found rather monodisperse NP size distributions. For the selected parameters, there are in total $N_{pol}^{tot} = m_{tot}/m_{pol} \approx 3.8 \times 10^{15}$ PS chains in the system ($m_{tot} = 10^{-4}$ g is the total mass of polymer in the feed stream, and $m_{pol} \approx 2.66 \times 10^{-20}$ g is the mass of a single PS chain). If all of the chains aggregate into NPs, there will be $N_{NP}^{tot} = N_{pol}^{tot}/N_{pol}^{NP} \approx 2.3 \times 10^{10}$ NPs, wherein each of them consists of $N_{pol}^{NP} = 4\pi R^3\rho_{PS}/3m_{pol} \approx 165\,000$ polymer chains, where $\rho_{PS}$ = 1.05 g/cm$^3$ is the density of PS. In the case of conditional thermodynamic equilibrium, however, only a fraction of



DOI: 10.1021/acs.langmuir.8b03399
Langmuir 2019, 35, 709−717

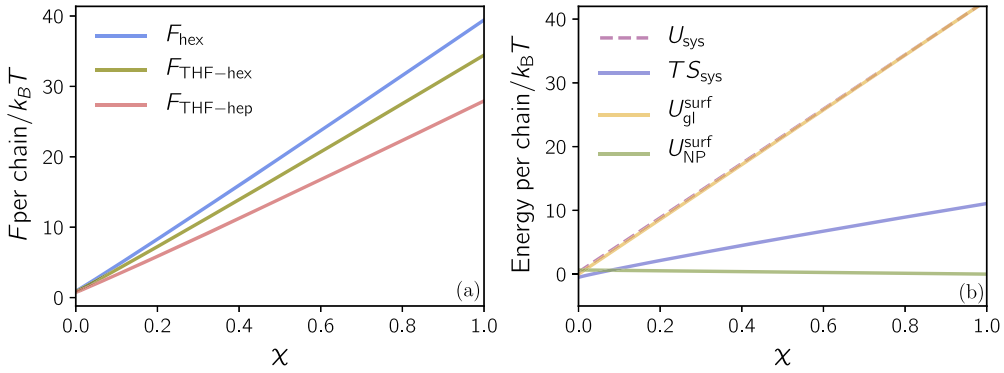


**Figure 9.** (a) Free energy per polymer $F/N_{pol}^{tot}$ of PS dispersed in THF−hexane, THF−heptane mixtures, and pure hexane vs the number fraction of free polymer globules in the system $\chi$. (b) Major contributions to the free energy, as indicated, vs $\chi$ in a THF−hexane mixture.

polymers aggregates into NPs and we denote the number fraction of free polymer globules in the system as $\chi = N_{pol}/N_{pol}^{tot}$.

The entropy of the system can be expressed as the sum of entropy of free globules and of NPs. The potential energy in the system is given by the NP−NP interaction $U_{NP-NP}$, the globule−globule interaction $U_{gl-gl}$, the NP−globule interaction $U_{NP-gl}$, the internal cohesion energy of a nanoparticle $U_{intra}$, and the surface energy with the surrounding medium, $U^{surf}$. A detailed derivation of these terms can be found in the Appendix of this manuscript.

Figure 9a shows the resulting free energy per polymer, $F/N_{pol}^{tot}$, versus the number fraction of free polymer globules in the system, $\chi$, for various media. From this plot, it is clear that the free energy decreases monotonically with decreasing $\chi$ and is minimized for $\chi = 0$, i.e., when the system consists solely of precipitated NPs. As a consistency check of our free-energy estimation, we have repeated this calculation for pure hexane, wherein we also find a minimum at $\chi = 0$, as expected. For pure hexane, the free energy per polymer is 0.9 $k_BT$ whereas we find a slightly smaller value of 0.8 $k_BT$ for the THF−hexane mixture and 0.7 $k_BT$ for the THF−heptane mixture.

The strongest potential energy per chain is in pure hexane, since surface energy dominates over other contributions in $U_{sys}$, and addition of a good solvent decreases the surface tension between the polymer and the solution. In Figure 9b, the most important contributions to the free energy $F$ are shown. The value of $U_{sys}$ is strongly dominated by the surface tension terms, namely, $U_{gl}^{surf}$ and $U_{NP}^{surf}$, with $U_{NP}^{surf} < U_{gl}^{surf}$, driving the system toward aggregation. The other contributions to the free energy $F$ are significantly smaller: $U_{gl-gl}$ is on the order of $10^{-5}$ $k_BT$ per polymer, $U_{NP-gl} \sim 10^{-7}$ $k_BT$ per polymer, $U_{NP-NP} \sim 10^{-9}$ $k_BT$ per polymer, and $U_{intra} \sim 10^{-1}$ $k_BT$ per polymer.

Finally, we also computed in the same fashion the free energy for the case when all globules form a single aggregate. Here, we find $F \approx 0.2$ $k_BT$, irrespective of the solvent composition, since the free energy is dominated by van der Waals interactions inside the aggregate and entropic contribution of chains in it. Surface tension plays only a secondary role, and thus the decrease in $\gamma$ in the solvent mixtures is negligible. The free energy per polymer is much smaller in the case of a single large aggregate compared to that in the dispersed systems with $R = 100$ nm NPs, indicating that the most preferable state is the formation of a single aggregate, when no stabilizing mechanism is present.

**Steric Stabilization.** To achieve steric stabilization of the NPs, the polymers at the surface of the aggregate need to stretch out into a thin layer of the solvent (mixture) surrounding the NP. The minimum thickness of this layer, $h$, can be estimated using the criterion that the thermal energy should outweigh the VDW attraction between two NPs at contact. With these considerations, we find

$$h > \frac{A_{131}R}{24k_BT} \tag{11}$$

where we used the simplified form of eq 1 for the case when $R_1 + R_2 \gg h$ and $R_1 = R_2 = R$ for the sake of simplicity. In eq 11 above, $A_{131}$ is the Hamaker constant for PS−(THF−hexane)−PS and PS−(toluene−hexane)−PS, respectively, which can be calculated using eq 2 in conjunction with the data provided in Table 1. We find that for the THF−hexane mixtures, the layer thickness increases from $h = 9.1$ nm for the 1:1:1 mixtures to $h = 9.8$ nm for the 1:1:10 mixtures. A similar trend is found for the toluene−hexane mixtures, with $h = 8.7$ nm for the 1:1:1 mixtures and $h = 9.7$ nm for the 1:1:10 mixtures. Given that the PS chains and the poor solvent (hexane or heptane) have similar solubility in the good solvent (THF or toluene),[55] we can safely assume that the good solvent is homogeneously distributed throughout the system. This picture is supported by previous experiments[56] and simulations,[57] wherein a good solvent was found enclosed in the NPs at a concentration similar to that of the surrounding solvent mixture. For the 1:1:1 mixtures, using THF and hexane, the solvent quality in the shell will then be slightly worse than that for the corresponding Θ-solvent,[58] where the end-to-end distance of the PS chains is $R_e \approx 9$ nm $\approx h$. For the other solvent compositions, however, the surface chains will be collapsed rather than stretched due to the poor solvent quality. Thus, according to these theoretical considerations, stable colloidal dispersions should only be feasible for the 1:1:1 mixtures, which agrees well with our experimental findings.

## CONCLUSIONS

We created polymeric nanoparticles with the flash nanoprecipitation technique, wherein a polymer solution is rapidly mixed with a miscible poor solvent to induce supersaturation and subsequent aggregation. In a majority of previous experiments, water was used as the poor solvent and the stability of the colloidal dispersion was attributed to water-induced surface-charging effects. To test this hypothesis, we used as the poor solvent hexane and heptane, which have a much smaller polarity than that of water. To our initial surprise, the precipitated nanoparticles were stable over many days. We theoretically investigated three possible explanations



DOI: 10.1021/acs.langmuir.8b03399
Langmuir 2019, 35, 709−717

for this stability, i.e., electrostatic stabilization, conditional thermodynamic equilibrium, and steric stabilization. Our experiments and considerations suggest that steric stabilization is most likely responsible for the particle stabilization in our experiments. However, electrostatic effects, such as residual water molecules adsorbing at the nanoparticle surface or polymer degradation, could also play a role in dispersion stabilization, since only a few elementary charges are, at least in principle, required to achieve stability. Unfortunately, reliable measurements of the $\zeta$ potential are challenging in the investigated nonpolar mixtures and so we cannot fully rule out electrostatic stabilization. Our experiments demonstrate that the fabrication of stable colloidal dispersions in nonaqueous media is also possible with FNP, allowing for a broader range of applications for this fabrication technique.

## EXPERIMENTAL METHODS AND MATERIALS

**Materials.** Polystyrene ($M_w$ = 16.0 kg/mol, $Đ$ = 1.03) was purchased from Polymer Source Inc. (Dorval, QC, Canada). Tetrahydrofuran, toluene, and hexane were purchased from Fisher Scientific, and heptane was purchased from Sigma-Aldrich.

**DLS and $\zeta$ Potential Measurements.** To measure the size and $\zeta$ potential of the particles, we used the Zetasizer Nano-ZS (Malvern Instruments, Malvern, U.K.). DLS measurements were performed in a glass cuvette, where 180 $\mu$L of NP suspension was dispersed in 1620 $\mu$L of a poor solvent, which was used in the fabrication process. One automatic measurement was made for each sample. $\zeta$ potential measurements were carried out using a combination of two techniques: phase analysis light scattering and mixed mode measurement (M3). The M3 technique consists of two steps, wherein the fast (FFR) and slow (SFR) reversal of the electric field are employed. During the FFR measurement, the mean value of the electrophoretic mobility is determined from particle thermal velocities. The distribution of the electrophoretic mobility is calculated during SFR measurement. Particle velocities are tracked for a longer time, but at this stage of the measurement, electro-osmosis can come into play. The electrophoretic mobility and its distribution are then obtained from subtracting results of the FFR measurement from the SFR measurement. Thus, the resulting $\zeta$-potential values are not affected by electro-osmotic effects, including electrode polarization. The measurements were performed in a glass cuvette with a dip cell, where 100 $\mu$L of NP suspension was dispersed in 900 $\mu$L of a poor solvent, which was used in the fabrication process.

**Titration.** The moisture content of the solvents was measured using a V20S Compact volumetric KF titrator (Mettler Toledo, Columbus, OH). Between 1 and 2.5 g of the solvent was weighed and quickly added to the titration vessel. The solvent was stirred for 5 min before titration began, and the water content reported by the KF titrator was expressed as % w/w. An Aquastar Titrant 5 was used as titrant with two-component reagents, and an Aquastar CombiMethanol was used as solvent (EMD Millipore, Burlington, MA).

**Sample Imaging.** Samples were prepared for transmission electron microscopy (TEM) by depositing multiple 10 $\mu$L drops of the colloidal suspension on a carbon-coated copper TEM grid (CF200-Cu, Electron Microscopy Sciences). The droplets spread beyond the TEM grid due to the low surface tension of the THF/heptane mixture, necessitating the use of multiple drops to get a reasonable concentration of particles on the grid.

**Solvent Evaporation.** A 5 mL sample of the colloidal suspension was placed on the rotary evaporator in a 20 mL scintillation vial. Evaporation was performed at 25 °C, rotating at 60 rpm pulling vacuum at 100 Torr for up to 90 min.

## Appendix

*Free-Energy Calculation.* We can write the entropy of the system as the sum of entropy of free globules and NPs, i.e., $S_{sys} = S_{gl} + S_{NP}$. The entropy of $N_{pol}$ free globules in the system can be estimated by the translational entropy of the chains in the reservoir

$$S_{gl} = k_B \ln \Omega_{gl} = k_B \ln \frac{(V_{res}/V_{gl})^{N_{pol}}}{N_{pol}!} \approx N_{pol} k_B \left( \ln \frac{V_{res}}{V_{gl} N_{pol}} + 1 \right) = k_B N_{pol} \left( \ln \frac{1}{\phi_{gl}} + 1 \right)$$

Here, we used Stirling's approximation $\ln N! \approx N \ln N - N$, and $\phi_{gl} = V_{gl} N_{pol}/V_{res}$ is the volume fraction of free globules in the system, with globule volume $V_{gl} = \frac{4}{3}\pi R_{gl}^3$. Further, we neglected the conformational entropy of the collapsed chains, since the monomers are rather close-packed and therefore contribute little to the overall entropy.

The entropy of $N_{NP}$ NPs can be expressed as a sum of the translational and conformational entropy of $N_{pol}^{NP}$ chains confined in a NP, in addition to the translational entropy of all NPs in the reservoir

$$S_{NP} = S_{NP}^{trans} + N_{NP}(S_{id}^{conf} + S_{id}^{trans}) \tag{12}$$

$$S_{NP}^{trans} \approx k_B N_{NP} \left( \ln \frac{1}{\phi_{NP}} + 1 \right) \tag{13}$$

$$S_{id}^{conf} = -\frac{3}{2} k_B N_{pol}^{NP} \tag{14}$$

$$S_{id}^{trans} \approx k_B N_{pol}^{NP} \tag{15}$$

where $\phi_{NP} = V_{NP} N_{NP}/V_{res}$ is the volume fraction of NPs in the system, with NP volume $V_{NP} = \frac{4}{3}\pi R^3$. The total entropy of the system is then given by

$$S_{sys} = \chi N_{pol}^{tot} k_B \left( \ln \frac{1}{\phi_{gl}} + 1 \right) + (1-\chi) N_{NP}^{tot} k_B \left( \ln \frac{1}{\phi_{NP}} + 1 - \frac{1}{2} N_{pol}^{NP} \right) \tag{16}$$

The potential energy of the system can be approximated as

$$U_{sys} = \chi^2 U_{gl-gl} + (1-\chi)^2 U_{NP-NP} + \chi(1-\chi) U_{NP-gl} + (1-\chi) U_{intra} + \chi U_{gl}^{surf} + (1-\chi) U_{NP}^{surf} \tag{17}$$

Here, $U_{gl-gl}$ is the potential energy due to the globule−globule interaction

$$U_{gl-gl} = 2\pi N_{pol}^{tot} \frac{N_{pol}^{tot}}{V_{res}} \int_{R_{gl}}^{\infty} U_{VDW}(A_{131}, R_{gl}, r) r^2 \, dr \tag{18}$$

the term $U_{NP-NP}$ is the potential energy due to the nanoparticle−nanoparticle interaction

$$U_{NP-NP} = 2\pi N_{NP}^{tot} \frac{N_{NP}^{tot}}{V_{res}} \int_{R}^{\infty} U_{VDW}(A_{131}, R, r) r^2 \, dr \tag{19}$$

and $U_{NP-gl}$ describes the nanoparticle−globule interaction energy

$$U_{NP-gl} = 2\pi \frac{N_{NP}^{tot} N_{pol}^{tot}}{V_{res}} \int_{R}^{\infty} U_{VDW}(A_{131}, R, R_{gl}, r) r^2 \, dr \tag{20}$$



DOI: 10.1021/acs.langmuir.8b03399
Langmuir 2019, 35, 709−717

The term $U_{intra}$ in eq 17 is the potential energy of chains within a NP, which can be estimated through

$$U_{intra} = N_{NP}^{tot} \sum_{i<j} U_{VDW}(A_{PS}, R_{id}, r_{ij}) \quad (21)$$

where the sum goes over all pairs of polymers $i$ and $j$ in a NP, $r_{ij}$ is the distance between them, and $R_{id} = R/(N_{pol}^{tot})^{1/3}$ is the radius of a chain inside of a NP. In this picture, each chain is effectively represented as a point particle within the confined NP volume and the interactions are governed by the VDW interaction with the Hamaker constant for pure PS, $A_{PS} = 6.4 \times 10^{-20}$ J.[16] To determine $U_{intra}$, we numerically computed the sum for multiple configurations, leading to $U_{intra}/N_{NP}^{tot} \approx -57\,600\ k_BT$ per NP. Alternatively, $U_{intra}$ can be estimated by computing the bulk energy density of a PS melt and then multiplying this value with the NP volume, $V_{NP}$. This approximation neglects surface effects of the spherical NP and gives a slightly higher energy of $U_{intra}/N_{NP}^{tot} \approx -59\,000\ k_BT$.

The contributions $U_{gl}^{surf}$ and $U_{NP}^{surf}$ in eq 17 are the surface energies of globules and NPs, respectively

$$U_{gl}^{surf} = N_{pol}^{tot} 4\pi R_{gl}^2 \gamma \quad (22)$$

and

$$U_{NP}^{surf} = N_{NP}^{tot} 4\pi R^2 \gamma \quad (23)$$

with surface tension $\gamma$. For PS in pure hexane, we can estimate the surface tension via $\gamma \approx (\gamma_{PS}^{1/2} - \gamma_{hex}^{1/2})^2$, with $\gamma_{PS} = 39.30$ mN/m for PS[59] and $\gamma_{hex} = 17.93$ mN/m for hexane.[39]

To calculate the surface tension $\gamma$ of the globules and NPs in the solvent mixtures, we used $\gamma_{THF-hex} = 19.13$ mN/m for a THF–hexane mixture with a 30% mole fraction of THF.[39] For a THF–heptane mixture with a 30% mole fraction of THF, a value of $\gamma_{THF-hep} = 20.58$ mN/m was measured.[39] To the best of our knowledge, the surface tension of toluene–hexane has not been reported yet but experimental measurements exist for toluene–heptane at a 25% toluene mole fraction, i.e., $\gamma_{tol-hep} = 20.56$ mN/m.[60] This value is rather close to the ones for the THF–hexane/heptane mixtures, and thus the free energies in the toluene–heptane mixtures should be comparable as well.

## AUTHOR INFORMATION


### Corresponding Author

*E-mail: ankouba@uni-mainz.de.

### ORCID

Tatiana I. Morozova: 0000-0003-3650-4772
Athanassios Z. Panagiotopoulos: 0000-0002-8152-6615
Robert K. Prud'homme: 0000-0003-2858-0097
Rodney D. Priestley: 0000-0001-6765-2933
Arash Nikoubashman: 0000-0003-0563-825X


### Notes

The authors declare no competing financial interest.

## ACKNOWLEDGMENTS

This work was supported by the National Science Foundation (NSF) Materials Research Science and Engineering Center Program through the Princeton Center for Complex Materials (DMR-1420541) and by the German Research Foundation (DFG) under the project number NI 1487/2-1.

## REFERENCES


(1) Wu, L.; Zhang, J.; Watanabe, W. Physical and Chemical Stability of Drug Nanoparticles. *Adv. Drug Delivery Rev.* **2011**, *63*, 456–469.
(2) Elsabahy, M.; Wooley, K. L. Design of Polymeric Nanoparticles for Biomedical Delivery Applications. *Chem. Soc. Rev.* **2012**, *41*, 2545–2561.
(3) Alvarez-Román, R.; Naik, A.; Kalia, Y.; Guy, R. H.; Fessi, H. Skin Penetration and Distribution of Polymeric Nanoparticles. *J. Controlled Release* **2004**, *99*, 53–62.
(4) Guterres, S. S.; Alves, M. P.; Pohlmann, A. R. Polymeric Nanoparticles, Nanospheres and Nanocapsules, for Cutaneous Applications. *Drug Target Insights* **2007**, *2*, 147–157.
(5) ShamsiJazeyi, H.; Miller, C. A.; Wong, M. S.; Tour, J. M.; Verduzco, R. Polymer-Coated Nanoparticles for Enhanced Oil Recovery. *J. Appl. Polym. Sci.* **2014**, *131*, No. 40576.
(6) Pearlstine, K.; Page, L.; El-Sayed, L. Mechanism of Electric Charging of Toner Particles in Nonaqueous Liquid with Carboxylic Acid Charge Additives. *J. Imaging Sci.* **1991**, *35*, 55–58.
(7) Solans, C.; Izquierdo, P.; Nolla, J.; Azemar, N.; Garcia-Celma, M. J. Nano-emulsions. *Curr. Opin. Colloid Interface Sci.* **2005**, *10*, 102–110.
(8) Higuchi, T.; Tajima, A.; Yabu, H.; Shimomura, M. Spontaneous Formation of Polymer Nanoparticles with Inner Micro-Phase Separation Structures. *Soft Matter* **2008**, *4*, 1302–1305.
(9) Johnson, B. K.; Prud'homme, R. K. Chemical Processing and Micromixing in Confined Impinging Jets. *AIChE J.* **2003**, *49*, 2264–2282.
(10) Derjaguin, B.; Landau, L. V. Theory of the Stability of Strongly Charged Lyophobic Sols and the Adhesion of Strongly Charged Particles in Solutions of Electrolytes. *Prog. Surf. Sci.* **1993**, *43*, 30–59.
(11) Overbeek, J. T. G.; Verwey, E. *Theory of the Stability of Lyophobic Colloids: The Interaction of Sol Particles Having an Electric Double Layer*; Elsevier Publishing Company, 1948.
(12) Van der Hoeven, P. C.; Lyklema, J. Electrostatic Stabilization in Non-Aqueous Media. *Adv. Colloid Interface Sci.* **1992**, *42*, 205–277.
(13) O'Brien, R. W.; Midmore, B. R.; Lamb, A.; Hunter, B. J. Electroacoustic Studies of Moderately Concentrated Colloidal Suspensions. *Faraday Discuss. Chem. Soc.* **1990**, *90*, 301–312.
(14) Nikoubashman, A.; Lee, V. E.; Sosa, C.; Prud'homme, R. K.; Priestley, R. D.; Panagiotopoulos, A. Z. Directed Assembly of Soft Colloids Through Rapid Solvent Exchange. *ACS Nano* **2016**, *10*, 1425–1433.
(15) Shchukin, E. D.; Pertsov, A.; Amelina, E.; Zelenev, A. *Colloid and Surface Chemistry*; Elsevier, 2001; Vol. *12*.
(16) Israelachvili, J. N. *Intermolecular and Surface Forces*; Academic Press, 2011.
(17) Santos, A. P.; Panagiotopoulos, A. Z. Determination of the Critical Micelle Concentration in Simulations of Surfactant Systems. *J. Chem. Phys.* **2016**, *144*, No. 044709.
(18) Gindy, M. E.; Prud'homme, R. K. Multifunctional Nanoparticles for Imaging, Delivery and Targeting in Cancer Therapy. *Expert Opin. Drug Delivery* **2009**, *6*, 865–878.
(19) D'Addio, S. M.; Prud'homme, R. K. Controlling Drug Nanoparticle Formation by Rapid Precipitation. *Adv. Drug Delivery Rev.* **2011**, *63*, 417–436.
(20) Pagels, R. F.; Edelstein, J.; Tang, C.; Prud'homme, R. K. Controlling and Predicting Nanoparticle Formation by Block-Copolymer Directed Rapid Precipitations. *Nano Lett.* **2018**, 1139–1144.
(21) Zhang, C.; Pansare, V. J.; Prud'Homme, R. K.; Priestley, R. D. Flash Nanoprecipitation of Polystyrene Nanoparticles. *Soft Matter* **2012**, *8*, 86–93.
(22) Sosa, C.; Liu, R.; Tang, C.; Qu, F.; Niu, S.; Bazant, M. Z.; Prud'homme, R. K.; Priestley, R. D. Soft Multifaced and Patchy Colloids by Constrained Volume Self-Assembly. *Macromolecules* **2016**, *49*, 3580–3585.
(23) Lee, V. E.; Sosa, C.; Liu, R.; Prud'homme, R. K.; Priestley, R. D. Scalable Platform for Structured and Hybrid Soft Nanocolloids by




DOI: 10.1021/acs.langmuir.8b03399
*Langmuir* 2019, 35, 709–717

Continuous Precipitation in a Confined Environment. *Langmuir* **2017**, *33*, 3444−3449.
(24) Grundy, L. S.; Lee, V. E.; Li, N.; Sosa, C.; Mulhearn, W. D.; Liu, R.; Register, R. A.; Nikoubashman, A.; Prud'Homme, R. K.; Panagiotopoulos, A. Z.; Priestley, R. D. Rapid Production of Internally Structured Colloids by Flash Nanoprecipitation of Block Copolymer Blends. *ACS Nano* **2018**, *12*, 4660−4668.
(25) Beattie, J. K.; Djerdjev, A. M. The Pristine Oil/Water Interface: Surfactant-Free Hydroxide-Charged Emulsions. *Angew. Chem., Int. Ed.* **2004**, *43*, 3568−3571.
(26) Beattie, J. K.; Djerdjev, A. M.; Warr, G. G. The Surface of Neat Water is Basic. *Faraday Discuss.* **2009**, *141*, 31−39.
(27) Vácha, R.; Rick, S. W.; Jungwirth, P.; de Beer, A. G.; de Aguiar, H. B.; Samson, J.-S.; Roke, S. The Orientation and Charge of Water at the Hydrophobic Oil Droplet−Water Interface. *J. Am. Chem. Soc.* **2011**, *133*, 10204−10210.
(28) Beattie, J. K.; Gray-Weale, A. Oil/Water Interface Charged by Hydroxide Ions and Deprotonated Fatty Acids: a Comment. *Angew. Chem., Int. Ed.* **2012**, *51*, 12941−12942.
(29) Vácha, R.; Marsalek, O.; Willard, A. P.; Bonthuis, D. J.; Netz, R. R.; Jungwirth, P. Charge Transfer between Water Molecules As the Possible Origin of the Observed Charging at the Surface of Pure Water. *J. Phys. Chem. Lett.* **2012**, *3*, 107−111.
(30) Roger, K.; Cabane, B. Why are Hydrophobic/Water Interfaces Negatively Charged? *Angew. Chem., Int. Ed.* **2012**, *51*, 5625−5628.
(31) Beattie, J. K.; Djerdjev, A. M.; Gray-Weale, A.; Kallay, N.; Lützenkirchen, J.; Preocanin, T.; Selmani, A. pH and the Surface Tension of Water. *J. Colloid Interface Sci.* **2014**, *422*, 54−57.
(32) Yan, X.; Delgado, M.; Aubry, J.; Gribelin, O.; Stocco, A.; Boisson-Da Cruz, F.; Bernard, F.; Ganachaud, F. Central Role of Bicarbonate Anions in Charging Water/Hydrophobic Interfaces. *J. Phys. Chem. Lett.* **2018**, *9*, 96−103.
(33) Delgado, Á. V.; González-Caballero, F.; Hunter, R.; Koopal, L.; Lyklema, J. Measurement and Interpretation of Electrokinetic Phenomena. *J. Colloid Interface Sci.* **2007**, *309*, 194−224.
(34) Xu, R.; Wu, C.; Xu, H. Particle Size and Zeta Potential of Carbon Black in Liquid Media. *Carbon* **2007**, *45*, 2806−2809.
(35) Russel, W. B.; Saville, D. A.; Schowalter, W. *Colloidal Dispersions*; Cambridge University Press, 1989.
(36) Lifshitz, E. The theory of molecular attractive forces between solids. In *Perspectives in Theoretical Physics*; Elsevier Ltd.: 1992, pp 329−349.
(37) Dzyaloshinskii, I. E.; Lifshitz, E.; Pitaevskii, L. P. General Theory of Van der Waals' Forces. *Phys.-Usp.* **1961**, *4*, 153−176.
(38) Singh, R. P.; Sinha, C. P. Dielectric Behavior of the Binary Mixtures of N-Hexane with Toluene, Chlorobenzene and 1-Hexanol. *J. Chem. Eng. Data* **1982**, *27*, 283−287.
(39) Piñeiro, Á.; Brocos, P.; Amigo, A.; Pintos, M.; Bravo, R. Surface Tensions and Refractive Indices of (Tetrahydrofuran+ N-Alkanes) at T = 298.15 K. *J. Chem. Thermodyn.* **1999**, *31*, 931−942.
(40) Shen, Y.; Goodwin, A. R.; Pirolli, L.; Marsh, K. N.; May, E. F. Determination of the Relative Permittivity, $\epsilon r$, of Heptane at Temperatures between (303 and 363) K and Pressures below 60 MPa with a Concentric Cylinder Capacitor at a Frequency of 1 kHz. *J. Chem. Eng. Data* **2013**, *58*, 2131−2135.
(41) Gill, D. S.; Singh, J.; Ludwig, R.; Zeidler, M. Nuclear Magnetic Resonance Relaxation, Permittivity, Viscosity and Ultrasonic Velocity Measurements in Binary Mixtures of Methanol and Tetrahydrofuran. *J. Chem. Soc., Faraday Trans.* **1993**, *89*, 3955−3958.
(42) El-Kashef, H. Study of the Refractive Properties of Laser Dye Solvents: Toluene, Carbon Disulphide, Chloroform, and Benzene. *Opt. Mater.* **2002**, *20*, 81−86.
(43) Oswal, S.; Gardas, R.; Phalak, R. Densities, Speeds of Sound, Isentropic Compressibilities, Refractive Indices and Viscosities of Binary Mixtures of Tetrahydrofuran with Hydrocarbons at 303.15 K. *J. Mol. Liq.* **2005**, *116*, 109−118.
(44) Looyenga, H. Dielectric Constants of Homogeneous Mixture. *Mol. Phys.* **1965**, *9*, 501−511.
(45) Prasad, M.; Strubbe, F.; Beunis, F.; Neyts, K. Space Charge Limited Release of Charged Inverse Micelles in Non-Polar Liquids. *Phys. Chem. Chem. Phys.* **2016**, *18*, 19289−19298.
(46) Smith, G. N.; Brown, P.; James, C.; Kemp, R.; Khan, A. M.; Plivelic, T. S.; Rogers, S. E.; Eastoe, J. The Effects of Counterion Exchange on Charge Stabilization for Anionic Surfactants in Nonpolar Solvents. *J. Colloid Interface Sci.* **2016**, *465*, 316−322.
(47) McGown, D. N. L.; Parfitt, G. D. Stability of non-aqueous dispersions. *Colloid Polym. Sci.* **1967**, *219*, 48−51.
(48) Morrison, I. D. Electrical Charges in Nonaqueous Media. *Colloids Surf., A* **1993**, *71*, 1−37.
(49) Parfitt, G. The Stability of Dispersions in Non-Aqueous Media. *Croat. Chem. Acta* **1970**, *42*, 215−221.
(50) Seth Roberts, G.; Wood, T. A.; Frith, W. J.; Bartlett, P. Direct Measurement of the Effective Charge in Ionpolar Suspensions by Optical Tracking of Single Particles. *J. Chem. Phys.* **2007**, *126*, No. 194503.
(51) Leunissen, M. E.; Van Blaaderen, A.; Hollingsworth, A. D.; Sullivan, M. T.; Chaikin, P. M. Electrostatics at the Oil-Water Interface, Stability, and Order in Emulsions and Colloids. *Proc. Natl. Acad. Sci. U.S.A.* **2007**, *104*, 2585−2590.
(52) Hsu, M. F.; Dufresne, E. R.; Weitz, D. A. Charge Stabilization in Nonpolar Solvents. *Langmuir* **2005**, *21*, 4881−4887.
(53) Hao, T. Exploring the Charging Mechanisms in Non-aqueous Multiphase Surfactant Solutions, Emulsions and Colloidal Systems via Conductivity Behaviors Predicted with Eyring's rate Process Theory. *Phys. Chem. Chem. Phys.* **2016**, *18*, 476−491.
(54) Yousif, E.; Haddad, R. Photodegradation and Photostabilization of Polymers, Especially Polystyrene: Review. *SpringerPlus* **2013**, *2*, 398.
(55) Burke, J. *Solubility Parameters: Theory and Application*; The Book and Paper Group of the American Institute for Conservation, 1984.
(56) Sosa, C.; Lee, V.; Grundy, L.; Burroughs, M. J.; Liu, R.; Prud'Homme, R. K.; Priestley, R. D. Combining Precipitation and Vitrification to Control the Number of Surface Patches on Polymer Nanocolloids. *Langmuir* **2017**, *33*, 5835.
(57) Morozova, T. I.; Nikoubashman, A. Coil-Globule Collapse of Polystyrene Chains in Tetrahydrofuran-Water Mixtures. *J. Phys. Chem. B* **2018**, *122*, 2130−2137.
(58) Baran, K.; Laugier, S.; Cramail, H. Investigation of molecular dimensions of polystyrene as a function of the solvent composition: application to liquid chromatography at the exclusion adsorption transition point. *Macromol. Chem. Phys.* **1999**, *200*, 2074−2079.
(59) Bender, G.; Gaines, G., Jr. The Surface Tension of Poly(styrene). *Macromolecules* **1970**, *3*, 128−131.
(60) Kahl, H.; Wadewitz, T.; Winkelmann, J. Surface Tension of Pure Liquids and Binary Liquid Mixtures. *J. Chem. Eng. Data* **2003**, *48*, 580−586.


DOI: 10.1021/acs.langmuir.8b03399
*Langmuir* 2019, 35, 709−717